Journal of Visualization, Vol. 3, No. 3 (2000) 253-265

Comparison of PIV Parameters Effects on Displacement Identification and Cross Correlation

Fayolle, J.*[1], Fournel, T.*[1] and Gervais, P.*[2]

*1 Laboratoire Traitement du Signal et Instrumentation, URA CNRS No. 842 Université Jean Monnet, 23, rue du docteur Paul Michelon 42023 Saint-Etienne Cedex, France.

*2 Centre de Thermique, INSA Lyon, URA CNRS 1372, batiment 404, 20, avenue Albert Einstein 69621 Villeurbanne Cedex, France.

Received 23 August 1999.
Revised 9 May 2000.

***Abstract*:** An algorithm is presented to determine displacements thanks to the identification method. Its main properties are described: no link with the particle size, measurement of the velocity distribution. Determination of effects of PIV parameters on displacement identification is made. Parameters used are noise, bias, velocity distribution. Therefore, we can define a validity domain of PIV parameters for identification and compare it with the domain of cross correlation. The identification validity range is based on 70% of isolated particles, on a displacement norm and on displacement gradients corresponding to less than half the size of the interrogation cell and to 10% of the average velocity. The comparison with cross correlation domains indicates that the cross correlation is more robust. However, the identification method is interesting because of the possibility of displacement distribution measurement. We use it to measure the decreasing of the turbulence intensity for a grid-generated turbulence.

***Keywords*:** particle image velocimetry, identification, displacement, signal to noise ratio.

***Nomenclature*:**

FFT : Fast Fourier Transform
s_1, s_2 : two successive and distinct synthetic PIV images, S_1, S_2 : FFT of s_1 and s_2 respectively
a : average displacement between s_1 and s_2
g : dispersion of displacement around a
h : impulse response of a stationary linear system, H : FFT of h
$\varphi_{s_1s_2}$: cross spectral density of s_1 and s_2, $\Phi_{s_1s_2}$: FFT of $\varphi_{s_1s_2}$
φ_{s_1} : spectral density of s_1, ϕ_{s_1} : FFT of φ_{s_1}
W : spectral window, FFT of Blackman's window
C : average number of particles per volume unit
SNR : Signal to noise ratio
%EV : percentage of erroneous vectors

1. Introduction

The local velocity measurement from two consecutive images of Particle Image Velocimetry (PIV) can be made by several methods. In high density PIV, cross-correlation is often used (Adrian, 1991). Another method uses an identification technique (Fayolle et al., 1995) to estimate the displacement in the studied area. The aim of this paper is to evaluate validity domains and accuracy of this method according to some PIV parameters. We compare

these validity domains to those of the cross correlation method.

In this study, PIV images are simulated by synthetic images. This way, we can generate an image sequence with only one varying parameter. Tested PIV parameters are density and size of particles used as marker, bias due to geometric limitation and laser sheet crossing (Prabel, 1985), average velocity and dispersion in velocity, particle luminescence; Adrian, noise. Each of these parameters is tested according to the accuracy of the displacement identification. This type of study has been already made for other techniques such as cross-correlation (Rouland, 1994; Keane and Adrian, 1992). Other parameters due to optic instrumentation have been studied independently of any measurement technique (Grant and Liu, 1989; Prasad et al., 1992).

We illustrate the use of displacement identification on a grid generated turbulence experiment. We estimate the decrease of the turbulence intensity in function of time and we compare it to the one obtained by cross correlation.

2. Identification: Notations and Properties

2.1 Displacement Identification

In our approach of the displacement in PIV (Fayolle et al., 1995) we consider that the two consecutive recordings s_1 and s_2 are respectively the input and the output of a stationary linear system (Fig. 1). Therefore, the displacement determination simply implies the determination of the system impulse response h.

Fig. 1. Displacement representation with a stationary linear system.

As the system input s_1 is fixed, the identification process uses the input-output correlation. Thus, the system impulse response is given by :

$$h = \mathrm{FFT}^{-1}\left[\frac{\boldsymbol{\Phi}_{s_1 s_2}}{\boldsymbol{\Phi}_{s_1}}\right] \tag{1}$$

with

$$\boldsymbol{\Phi}_{s_1 s_2} = \boldsymbol{S}_1^{*}\boldsymbol{S}_2 \text{ and } \phi_{s_1} = \left|\boldsymbol{S}_1\right|^2 \tag{2}$$

For computing time and noise reduction, we use a smoothed estimation of spectral densities (as opposed to the simple estimation of spectral densities used by Okuno and Kinoshita, 1987, Okuno, 1991a and 1991b). Indeed, the use of a smoothed estimation of spectral densities eliminates problems due to spatial limitations of signals and therefore it erases secondary harmonics of displacement peaks. The use of a smoothed estimation of spectral densities is essential because it induces noise reduction and an easier detection of displacement peaks. In many cases, peak detection, which is not possible otherwise, becomes possible. Here, the smoothed estimation is realized thanks to a Blackman window w. However, other windows, such as Hamming, Bartlett or Hanning windows, lead to the same results. The choice of a Blackman window is interesting because its discrete Fourier Transform W is not nil only on a 5×5 neighborhood of the origin.

Therefore, the determination of displacement by use of an identification method can be given by:

$$h = \mathrm{FFT}^{-1}\left[\frac{(S_1^{*}S_2) * W}{\left|S_1\right|^2 * W}\right] \tag{3}$$

We should emphasize here differences between identification and cross correlation. Usually, the cross correlation CC in PIV is obtained by:

$$CC = \mathrm{FFT}^{-1}\left[\frac{S_1^* S_2}{|S_1||S_2|}\right] \tag{4}$$

Without the Blackman window, the definitions of identification and cross correlation are almost similar. Let us explain mathematically the differences for the ideal displacement case. With the ideal displacement hypothesis, the second image can be expressed as:

$$s_2(x,y) = s_1(x - a_x, y - a_y) \tag{5}$$

Then, their Fourier transform are linked:

$$S_2(\xi,\eta) = S_1(\xi,\eta)\,\exp\left(-2i\pi(a_x\xi + a_y\eta)\right) \tag{6}$$

Therefore, the identification and the cross correlation are given by the two following expressions:

$$h = \mathrm{FFT}^{-1}\left(\exp\left(-2i\pi(a_x\xi + a_y\eta)\right)\right) = \delta(a_x, a_y) \tag{7}$$

$$CC = \mathrm{FFT}^{-1}\left[\frac{S_1^* S_1}{|S_1||S_2|}\exp\left(-2i\pi(a_x\xi + a_y\eta)\right)\right] = \delta(a_x, a_y) * \mathrm{FFT}^{-1}\left[\frac{S_1^* S_1}{|S_1||S_2|}\right] \tag{8}$$

Thus, the difference between the two approaches becomes clear. In the case of an ideal displacement, the identification result is a Dirac distribution corresponding to the displacement. On the contrary, the cross correlation result is the convolution of the same Dirac distribution with an energy term. This last term corresponds to the relative energies of the two signals and therefore it depends on the shape and the luminescence of the particles.

We explain now the differences between the two approaches in a qualitative manner. The differences between the identification and the cross correlation were the use of different denominator and smooth window. Let us discuss first about the denominator difference. The cross correlation denominator is simply a normalization term, whereas, for the identification, the ratio corresponds to a deconvolution made in the Fourier space. The numerator term is similar in both cases and contains a peak, which determines the displacement. Thus, all the difference between the two approaches lies in the denominator. For the cross correlation, normalization is made to eliminate problems coming from energy difference between frames. For identification, the denominator corresponds to a deconvolution and it allows the elimination of the particle size parameter (cf. Section 2.2).

Another difference lies in the use of smoothed estimations of spectral densities as we discussed earlier. The use of a window is not theoretically essential and the difference between Okuno's technique and our technique is this treatment of the Fourier function. However, the use of a window function improves the quality of the detection of the displacement peak. In few cases, the use of a window allows the measurement of the displacement (cf. Figs. 2(c), 2(d) and 3(c), 3(d)). The Blackman window plays very big important role on the identification since it neglects the high frequencies. The comparison between Figs. 2(c) and 2(d) on one hand and 3(c) and 3(d) on the other hand illustrates this phenomenon. Indeed, the result obtained by the identification without Blackman window

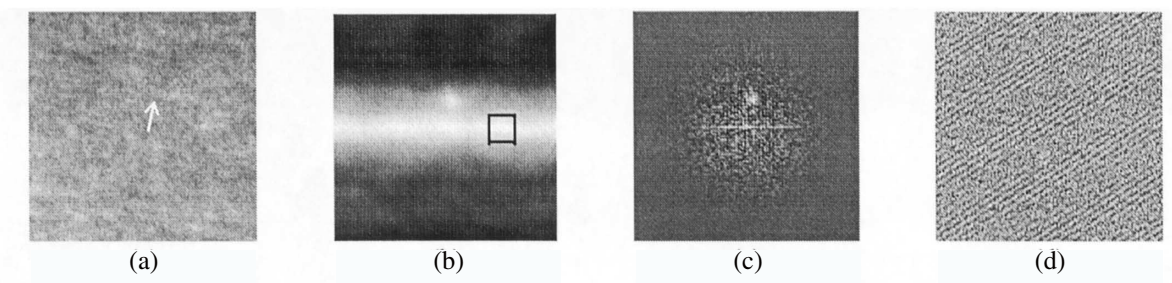

Fig. 2. (a) 128 128 sub image (im18) of the Europiv image database (comprising a vertical light deviation), (b) its cross correlation, (c) its identification with Blackman window and (d) its identification without Blackman window. The real particles displacement is marked on (a) and the cross correlation maximum is marked on (b).

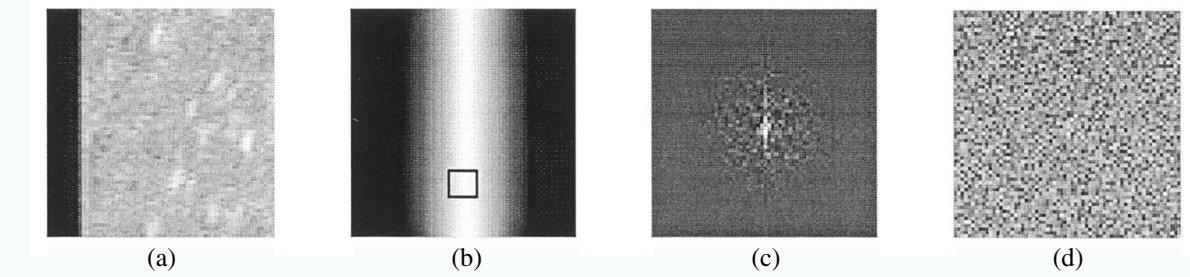

Fig. 3. (a) 64 64 sub image with a piece of the facilities edge, (b) its cross correlation, (c) its identification with Blackman window and (d) its identification without Blackman window. The particles displacement is marked on (a) and the cross correlation maximum is marked on (b).

is disturbed by high frequency noise. This noise is simply due to the numerical sampling of the images. On the contrary, the use of a Blackman window erases these high frequencies and then the displacement peak can be localized.

The consequence of these different approaches of the displacement measurement can be shown in real cases (Figs. 2 and 3). On Fig. 2, the cross correlation fails because there is a light deviation in the sub image. On the contrary, displacement identification is not sensitive to this parameter and the displacement is measured (Fig. 2(c)). On Fig. 3, cross correlation fails because a piece of the facilities edge is present in the sub image. Such conditions are not favourable to obtain the displacement by superposition (Fig. 3(b)). But, they do not prevent us from finding the frequency linked to the displacement: identification succeeds (Fig. 3(c)).

2.2 Main Properties

In the case of an ideal displacement a, the system modeled on Fig. 1 is simply a convolution product with a Dirac distribution δ_a. Therefore, the impulse response of this system is δ_a. The interpretation in terms of PIV induces a main property of the identification method. If all the markers seeded in the fluid have the same velocity, the second recording is a shifted version of the first one (Thus, it is the case of an ideal displacement). Thus, the result of displacement identification is a one-pixel size peak, (corresponding to the Dirac distribution δ_a,) independently of the marker size. If we compare the cross correlation and the identification peaks (Fig. 4), we see that only the first one is linked to the particle size (these results are obtained from real flow fields seeded with particles (Rilsan) of diameter 80 μm corresponding to particle-image size of 2 or 3 pixels).

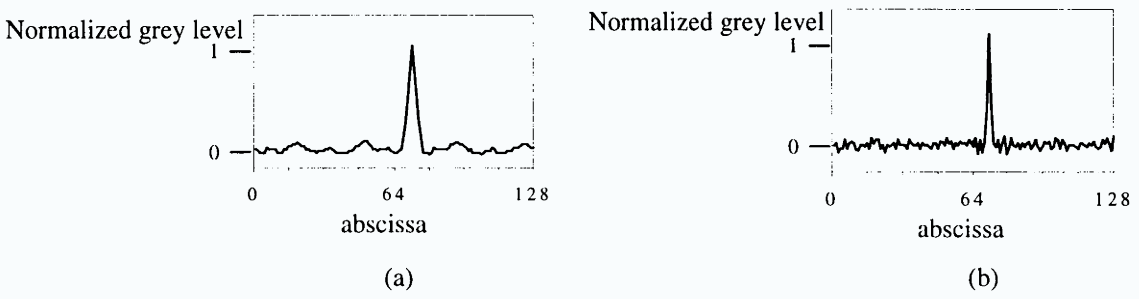

Fig. 4. Normalized horizontal profile of (a) cross correlation peak and (b) identification peak.

Moreover, if the displacement between the two successive frames is not perfectly uniform but disturbed, the impulse response of the linear system can be written as:

$$\boldsymbol{h} = \delta_a * \boldsymbol{g} \tag{9}$$

Therefore, the determination of this response by the identification method restores not only the average displacement a, but also the displacement distribution g around a. As an illustration of this method feature, we have simulated the displacement of a particle set with an asymmetric distribution g as shown on Fig. 5 (b). The

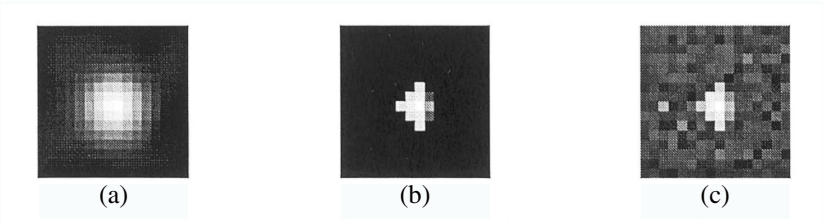

Fig. 5. (a) Cross correlation peak, (b) asymmetric displacement distribution and (c) identification peak.

cross correlation and identification methods give the average displacement, but only the identification peak gives back the shape of the velocity dispersion (Figs. 5(a) and 5(c)).

Moreover, since we know the velocity distribution in the sub image, we can compute an average velocity with a sub-pixel precision. And this precision is not obtained thanks to a fitting or an interpolation (as it is the case for cross correlation) but it is simply an average of all particles displacements. In order to simplify this explanation, let us consider a 1D case and an ideal displacement. If the displacement norm is not a multiple of 1 pixel, then the identification peak has two modes as it is shown on the scheme below.

The correct displacement is given by a weighted average of the displacement peaks. In our example, the real displacement is given by :

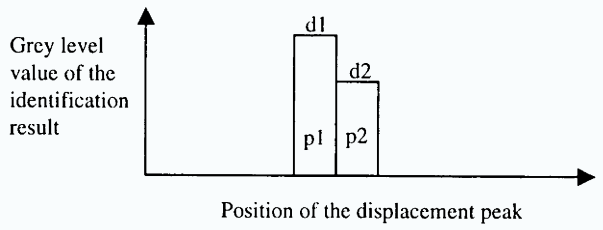

Fig. 6. Synthetic representation of an identifcation peak corresponding to a sub-pixel displacement. p_1 and p_2 represent the position of the pixels around this sub-pixel displacement whereas d_1 and d_2 are the values of the displacement peak respectively at p_1 and p_2.

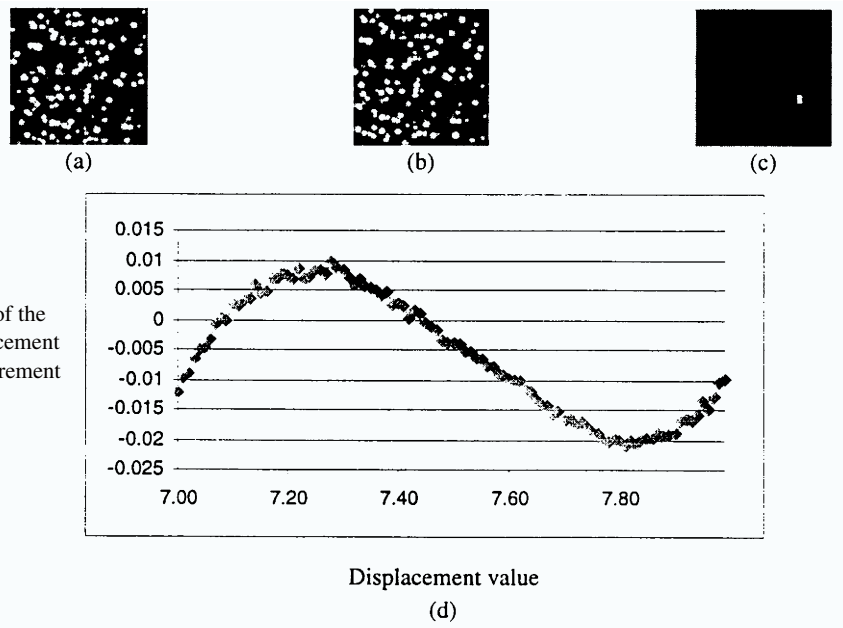

Fig. 7. (a-b) Two images of particles with an ideal displacement of (7.1, 3.6) between them, (c) identification result (zoom in by a factor 2) and (d) error of the sub-pixel measurement for displacements ranging in [7.0, 8.0] by step of 0.01 pixel.

$$d = \frac{d_1 p_1 + d_2 p_2}{p_1 + p_2} \tag{10}$$

To illustrate this measurement, we have simulated two images corresponding to an ideal displacement of (7.1, 3.6) pixels. Figure 7 shows these two images and the identification result. The weighted average of the displacement peaks gives a displacement of 7.10 pixels horizontally and 3.58 pixels vertically. Another test is made to prove this ability. We have simulated different sub-pixel displacements ranging in [7.0, 8.0] by step of 0.01 pixel. The identifcation method is used to measure each of these displacements. Then, we evaluate the error made through the norm of the difference between the correct and the measured displacements. This result is shown in Fig. 7(d). The average error is equal to 0.0097 pixel. Therefore, the ability of sub-pixel measurement by identification is proved.

A third property of the method is its no-link with any difference in particle luminescence during each of the two PIV recordings. This is obvious if we consider Eq. (1). If the first frame s_1 is multiplied by a real constant λ, when we applied the Fourier transform linearity, we obtain uniformly the response h divided by λ. On the contrary, if the second frame is multiplied by λ, the impulse response is also multiplied by λ. But in all cases, it only changes the dynamic of h and not its features: the peak size is 1 pixel and we measure the displacement distribution.

In the case of the cross correlation computed with discrete Fourier Transform, such modifications do not change the shape of the peak. Moreover, they do not change the peak amplitude.

3. Model of Main PIV Parameters

3.1 Presentation

The no-link between the particle size and the identification peak size allows us to eliminate the particle size from the PIV parameters list. Each remaining parameter will be tested independently on a set of synthetic images. The main parameters are:

- particle concentration,
- geometric and luminescence bias,
- ratio between size of interrogation cell and average velocity,
- ratio dispersion over average velocity,
- noise.

The geometric bias due to the limitation of the interrogation cell is here named XY bias (or in plane loss of correlation). We name as Z bias (or out of plane loss of correlation) the luminescence bias that occurs when the flow is three dimensional, i.e. when particles cross the laser sheet.

The validity domain of the method for the current varying parameter is evaluate through the variation of a signal to noise ratio (SNR) defined as :

$$\mathrm{SNR} = \frac{p - \mu_n}{\sigma_n} \tag{11}$$

where p is the peak magnitude, μ_n is the average of noise and σ_n its standard deviation. In the diagrams, we refer to the SNR of the identification peak as $\ll$SNR_I$\gg$ and $\ll$SNR_C$\gg$ for the cross correlation.

3.2 Parameters Model

According to Adrian (1991), we determine the average number of particles per unit volume named *C*. Particles are modeled by randomly distributed points. The particle size used in this simulation is 1 pixel. This choice is due to the absence of link between the method and the particle size. With this choice, we control the particle concentration precisely. The position of particles follows a uniform distribution in the area defined by the laser sheet. In the third direction (z axis), the non uniform luminescence of the laser sheet is represented by means of a gaussian grey level. We choose for the average and the standard deviation of this gaussian distribution 0 and 1/3 respectively. With this choice, 99.73% of the particles has a z position ranging from -1 to $+1$.

We should comment here the choice of 1 pixel particle size. Indeed, for the cross correlation, when the area of one particle image has several pixels, the results are a little bit better. However, the difference between grey levels of particles allows us to eliminate correspondence ambiguities. Thus, the effect of this choice is not so

important and we can admit it.

To test the effect of the concentration on displacement identification, we generate a set of image couples with different concentrations. For one couple, the second image is a shifted version of the first one (the shift corresponds to an ideal displacement). Because of geometric limitation of interrogation cells, particle positions can not be chosen everywhere in the cell. By keeping two seedless strips, we ensure that every particle in the first image is associated with another particle in the second image. The strip size is equal to the absolute value of the displacement in each direction. This way, we do not introduce isolated particles and we test only the influence of particle concentration.

If particles are uniformly distributed over all the interrogation cell of the first image, there are some particles without any duplicate in the other image. The amount of XY bias due to geometric limitation is limited by the particle concentration. Indeed, this proportion is directly related to the ratio between the area of the two seedless strips and the cell area. If the particle concentration increases, the XY bias increases too. Therefore, to test the XY bias effect, we take the same set of images as previously, but the choice of particle positions is allowed everywhere in the cell.

The Z bias due to the luminescence derive or to three dimensional phenomenon (particle crossing the laser sheet) is modeled by a given number of isolated particles. These isolated particles are uniformly distributed over the entire cell. To increase the influence of this parameter, we increase the rate of isolated particles.

To test the importance of the displacement norm on results, we generate a set of image couples with different shifts. The shift starts with a minimal size (one pixel) and increases of one pixel each time, this corresponding to each couple, until half the size of the cell. Values of displacements are given as percentages of the maximum displacement. It may be possible that the displacement direction has an effect on results. Choosing different displacement directions (x axis, y axis, diagonal or other) and comparing results makes the illustration of this effect.

In real PIV images, there is always a velocity distribution around the average velocity. Therefore, if we want to approach real PIV images, the second image of every couple must not be a shifted version of the first one but an average shifted version. To do so, we consider a histogram of displacement distribution. Gradient effects are linked mainly to the size of this distribution and not to the distribution values. Therefore, the parameter is the size of the histogram. Thus, if we have a histogram size equal to $a \times b$ pixels, it means that :

$$\frac{-a}{2} \le \frac{\partial u}{dx} \Delta t \le \frac{a}{2} \text{ and } \frac{-b}{2} \le \frac{\partial v}{dy} \Delta t \le \frac{b}{2} \tag{12}$$

where u and v are the displacement components along each axis expressed in pixels and Δt the exposure time delay. To measure the gradient effect, a set of image couples is generated with gaussian distribution histograms of displacements with different sizes. We start with a histogram size of 1×1 pixels and we increase it of 1×1 pixels each time until we reach one-third of the cell size. Moreover, the result is probably linked not only to the histogram size but also to the ratio between the displacement norm and the histogram size. To show that, we do a simulation with a given size of the histogram (for example 3×3 pixels) and a varying displacement norm. The SNR variation tells us if the identification results are linked to these two PIV parameters.

The last PIV parameter we model is the noise. There are two types of noise: sampling noise and optical noise. We have chosen not to take into account the first one, which is linked to the recording system. The noise due to optic instrumentation is well represented by the recording of a dark image, i.e. an image of the laser sheet with no seeding. We record two images of that kind, and we add them respectively to each image of each couple. This addition is made exclusively where there are no particles. Indeed, on a particle spot, the camera has a useful signal, which should not be disturbed in good conditions. On the contrary, if there is no particle spot, there is no useful signal for the camera, and the grey level is strongly linked to the optic instrumentation noise. For our tests, we start with noise amplitude corresponding to 1% of the particle maximum luminescence and we progress of 1% each time until 100%.

4. Results for Identification Method

In this section, we present results of the identification method according to the variation of different PIV parameters presented above. For each value of one PIV parameter, the measurement of SNR variations is an average over 32 samples (a set of 32 samples is constituted of 32 image couples with same PIV parameters). The

sampling theory indicates that, over 30 samples, the sampling distribution of averages is very nearly normal even if the population is not normal (Spiegel, 1961). Therefore, we estimate that the measurement is representative. On each graph presented below, the left column refers to the SNR and the right column to the percentage of erroneous vectors (%EV).

First, we test the concentration effect. An ideal displacement (7×3 pixels) and an interrogation cell size (32×32 pixels) are chosen. The number C of particles belonging to each interrogation cell varies from 1% to 68% of the cell area. The ratio between the bias strips and the cell area induce this upper limit (68%). The strips of XY bias are seedless to eliminate isolated particles. With the displacement chosen above, it corresponds to strips of 7 pixels and 3 pixels width in each direction. The reservation of two strips to eliminate the XY bias is a hypothesis which is obviously not correct for real flow field. However, we make this hypothesis to test independently the effect of concentration.

The number of erroneous vectors is always zero independently of the concentration. Furthermore, the SNR is constant and high (Fig. 8). The case of 0% concentration is obviously not addressed and the lower concentration (1%) corresponds to the case of 1 particle per sub image.

If the two strips of XY bias are not reserved, the results do not change a lot. The SNR variations are similar (Fig. 9). The SNR is divided by a constant as seen above. This is due to the preservation of the proportion of isolated particles (XY bias) even though the concentration varies. This proportion is equal to the ratio between the strips and the cell area.

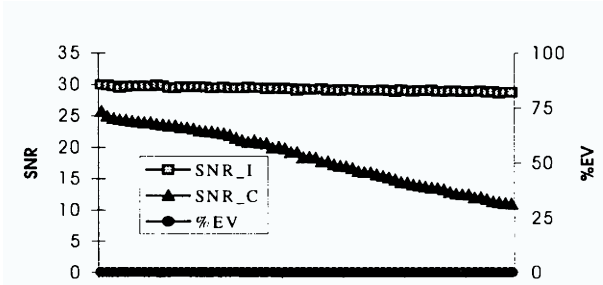

Fig. 8. SNR variation according to particle concentration C.

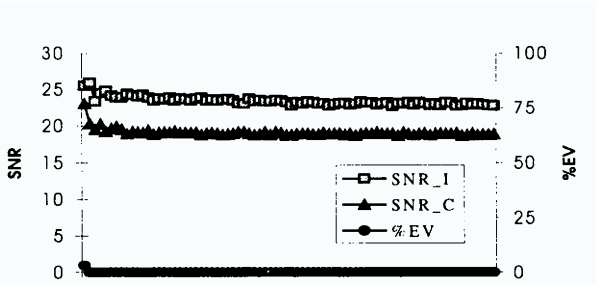

Fig. 9. SNR variation according to particle concentration with XY bias.

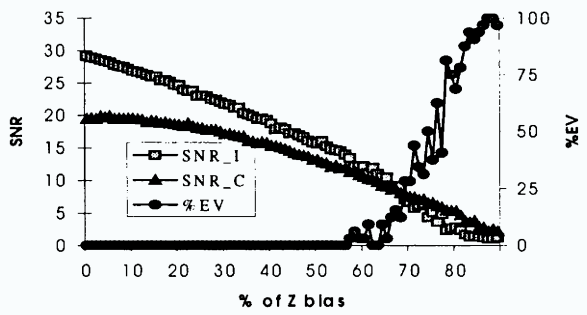

Fig. 10. SNR variation according to Z bias amount.

The presence of isolated particles due to three-dimensional phenomenon deteriorates this excellent result. But if the number of isolated particles is less than 65% of the total number, the identification always gives the correct result (Fig. 10). For upper values of this rate, there are some erroneous vectors. The SNR decreases linearly in function of the Z bias amount and reaches its lower bound (which is 1) around 85% of isolated particles.

To test the displacement norm and direction effect, we choose four directions: (1,0), (0,1), (1,1) and (2,1). For each of these directions, we generate image couples. The displacement ranges from 1 pixel to the maximum displacement in the given direction (for example, half the cell size along one axis). We present results in function

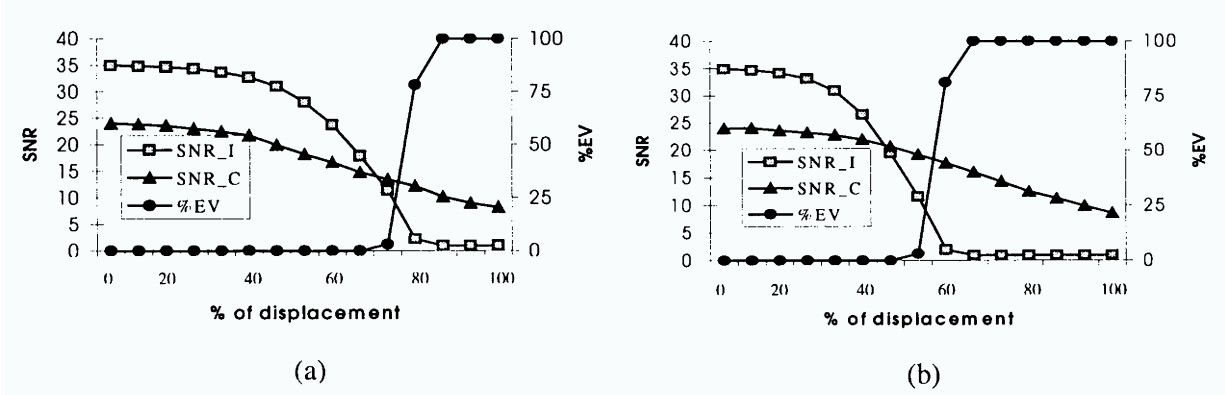

Fig. 11. SNR variation according to the percentage of displacement along (a) one axis and (b) one diagonal.

of displacements expressed as a ratio of the maximum displacement. First, we simulate displacements along an axis (x or y). Identification results are satisfactory until a displacement corresponding to 73% of the maximum displacement (Fig. 11(a)). Along the diagonal, this limit decreases to 53% (Fig. 11(b)). And if we consider the intermediary direction, results are good for a displacement less than 71% and they are very similar to the case of an axial displacement. Therefore, we conclude that the worst case is a displacement along one diagonal.

However, these results must be weighted by the absence of isolated particles (in particular, there is no XY bias). If we allow the presence of isolated particles, the percentage of the maximum displacement for which the identification gives the correct displacement decreases (66% instead of 73% along the axis).

To determine the robustness of the method on a real application, it is important to test the gradient effects. We choose arbitrarily Gaussian distribution as velocity distribution. On a 32×32 pixels cell, the correct displacement is not restored by the identification method for a velocity distribution strictly larger than 2×2 pixels (i.e. $\partial u/\partial x \ \Delta t$ and $\partial v/\partial y \ \Delta t$ not greater than 1 pixels) which corresponds to 13% of the cell size (Fig. 12(a)). If this cell size is now 64×64 pixels, then the upper convenient distribution is double. These tests are realized with an average concentration. However, the concentration value has no effect on the obtained results. On the contrary, if the displacement norm decreases, results improve greatly (Fig. 12(b)). Indeed, the results shown on Fig. 12(a) are obtained with a displacement corresponding to 50% of the maximum displacement. If we start again the same tests with a displacement of 14%, the identification method allows to restore the correct shift for distributions less than 4×4 pixels (i.e. $\partial u/\partial x \ \Delta t$ and $\partial v/\partial y \ \Delta t$ less than 2 pixels) instead of 2×2 pixels (Fig. 12(b)). For lower sizes of the displacement, results are turned off by noise located at the cell center. This arises because of the lower value of the displacement norm.

Now, we fix the velocity distribution size to 4×4 pixels (i.e. $\partial u/\partial x \ \Delta t$ and $\partial v/\partial y \ \Delta t$ equals to 2 pixels), and we make the displacement norm vary from 6% to 66% of the maximum displacement. With this configuration, we can determine the upper limit of displacement for which identification results are good in

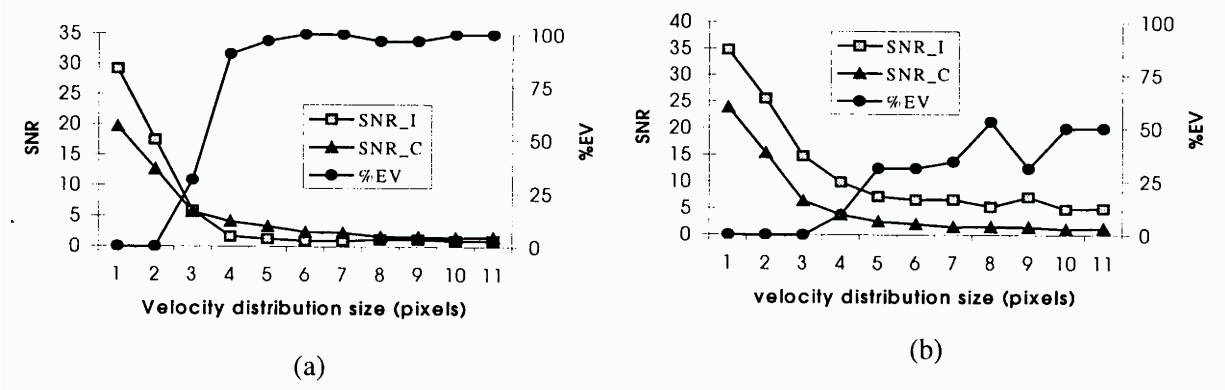

Fig.12. SNR variation according to velocity distribution size (a) cell interrogation: 32 32 pixels, displacement : 50% and (b) cell interrogation: 32 32 pixels, displacement: 14%.

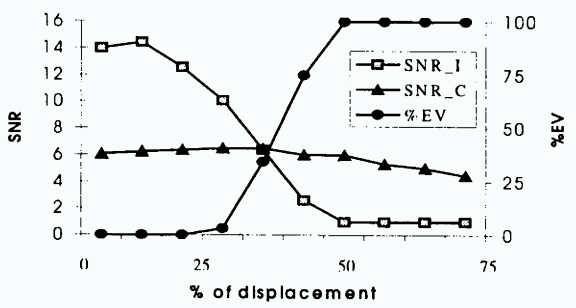

Fig. 13. SNR variation according to the percentage of displacement with 4 4 pixels velocity distribution.

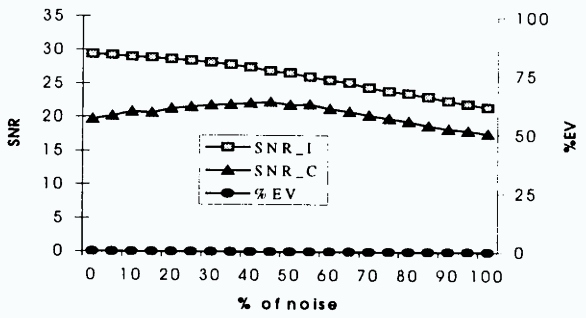

Fig. 14. SNR variation according to noise (without Z bias).

presence of gradients (Fig. 13). For the above values, this limit appears to be around 27%. If the dispersion size increases to 5×5 pixels, this displacement limit decreases to 13%.

Finally, noise addition on one or both images does not disturb the detection of the correct peak. Indeed, even if the noise and the particles luminescence are equivalent, i.e. noise corresponding to 100% of particle luminescence, the peak SNR remains high (Fig. 14). Moreover, the percentage of erroneous vectors is constant and nil. These tests are realized with no isolated particles. But, if we introduce a percentage of Z bias, the correct displacement is still determined. The consequence is a uniform decrease of the SNR.

5. Comparison with Cross Correlation

We present here a comparison of the previous results with validity domains of cross correlation. We compute on the same couples of images the cross correlation instead of the displacement identification and we apply the same test procedure. We give below the main results of this comparison (Fayolle, 1996).

For the concentration parameter, Figure 8 shows that the SNR of the cross correlation peak decreases when the concentration increases (unlike the identification). Indeed, the number of false cross couples of particles increases two times more than the correct couples. The model of displacement used for the identification does not care at this ratio, on the contrary the cross correlation is strongly linked to it.

If we allow geometric bias, this effect disappears (because of a statistical effect due to the periodisation intrinsic to the calculus of the Fourier transform) (Fig. 9).

For the luminescence bias parameter, the cross correlation SNR decreases in the same way as the identification one but the slope is less important in the cross correlation case (Fig. 10). Moreover, in this case, the SNR does not reach its lower bound. Therefore, the identification is more sensitive to this parameter than the cross correlation.

We have seen (Fig. 11) that the identification can not measure large displacements (over 60 or 70% of the cell interrogation size). On the contrary, there is no maximum for the displacement which can be measured by the cross correlation method. In both cases, the decrease of the SNR is due to the increase of the zone of the geometric bias. But, for cross correlation, the covering between the two exposures is always important enough to allow the displacement measurement. Indeed, for a displacement of 100%, half of the cell is still not biased.

Behaviors of correlation and identification methods according to gradient effect are quite similar. Indeed, although the identification SNR is greater than the cross correlation one, the gradient limit is identical in both cases. $\partial u/\partial x \quad \Delta t$ and $\partial v/\partial y \quad \Delta t$ are equals to 2 pixels for a little displacement (Fig. 12(b)) and 1 pixel for an upper one, in both cases (Fig. 12(a)). If we fix the gradient value to this limit (distribution of 4×4 pixels), we can measure the larger displacement in the cell by cross correlation. Whereas we can not measure displacements over 27% of the cell size by the identification method (Fig. 13). This result confirms the previous one on the sensibility of the identification to the displacement norm.

The presence of noise does not disturb the displacement measurement for both methods (Fig. 14). If we fix the noise level to its maximum, i.e. the level of particle luminescence, we can define in noisy images the minimal concentration possible for displacement measurement (Fig. 15). This minimal concentration is equal to 6% for the identification and 4% for the cross correlation.

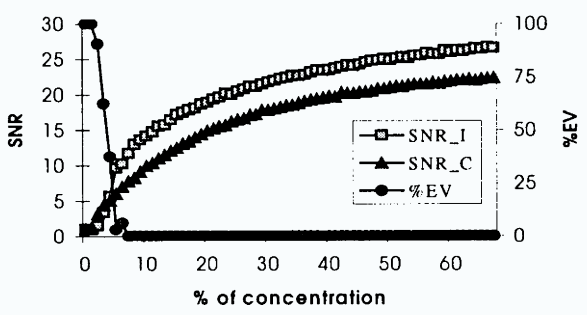

Fig. 15. Determination of the minimal concentration necessary for measurements in noisy images.

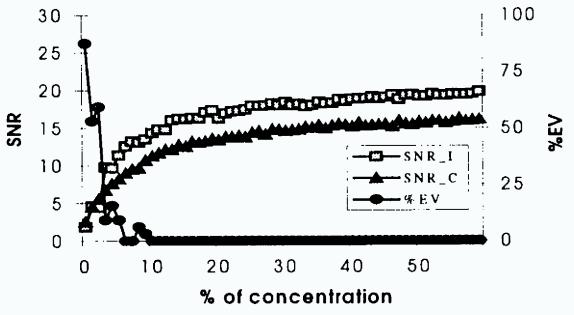

Fig. 16. SNR variation according to particle concentration in a ≪real case≫ (with Z bias, noise and presence of gradient).

Finally, we try to simulate a real flow seeded with different concentrations. We fix the Z bias at the same proportion (25%) of the particle concentration. The XY bias strips are not reserved (as it is always the case in real flow). The noise is fixed at 50% of the particle luminescence. The gradient of displacements corresponding to $\partial u/\partial x \quad \Delta t$ and $\partial v/\partial y \quad \Delta t$ equals to 2 pixels. The concentration varies from 1% to 60% of the area of the studied field. The result is shown on Fig. 16. The behavior of the two methods is similar to the previous case. The change is a decrease of the limit values of the SNR. Consequently, we conclude that the identification method is useful for displacement measurements in real flow field: the SNR of our method is greater than the cross correlation one even in real situations.

The various comparisons studied above allow us to see that cross correlation is more robust. But, the range of the identification is large enough to assure its usefulness in real experiments. Thus, if we belong to both validity domains, the use of the identification is more interesting because it allows the measurement of the displacement distribution around the average displacement. Furthermore, the measurement of the average velocity is made with a best SNR.

6. Application

We present in this section an example of displacement measurement by the identification method for a real experiment. The experiment chosen is the study of a grid-generated turbulence. The grid thread is 4 cm with bars of 1 cm. The grid goes down in a water tank at a speed of 30 cm/s. The Reynolds number is 12,000. We are interested by the variation of the standard deviation of displacements during the experiment. The aim is to obtain a decreasing rule of this standard deviation and to verify the empirical law proposed by Comte-Bellot and Corrsin in 1966.

To do that, we record images with a CCD camera at a speed of 25 images per second with a resolution of 768×576 pixels. This resolution corresponds to a field of 9×9 cm. The scheme used is to compute a complete field of displacements for each image couple and for each realisation of the experiment with both methods. (This represents over 500 Megabytes of images.) Then, we consider all the displacement vectors as a statistic population. We compute the standard deviation of this statistic population. The population consists of more than 400 instantaneous displacement vectors. We report the standard deviation value on a diagram in function on time (between 1 second and 7 seconds). We obtain curves presented Fig. 17. These curves follow a power rule with a coefficient 1.298 for the identification and 1.32 for the cross correlation. For both methods, this result conforms with the empirical law (power rule with a coefficient 1.3). Moreover, the iteration of this scheme on other realisations of the experiment (up to 13 realisations) gives the same results.

This experiment is a validation of the identification method in a real situation. Indeed, according to the cross correlation results, the identification curve is smoother and closer to the theoretical variation of the turbulence intensity determined from experiment features (Fig. 17). The cross correlation measurements are made with sub-pixel precision (the interpolation technique used is to fit a gaussian on a 3×3 neighbourhood of the displacement peak).

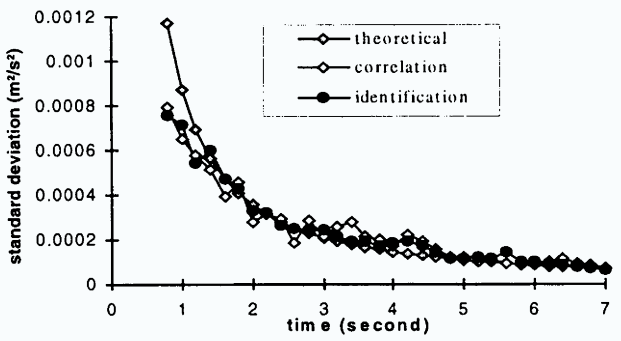

Fig. 17. Variation of the standard deviation of displacements in grid turbulence. Displacements are measured by the identification method.

The both techniques had relatively larger error at 1 second. This is not due to a systematic error in the experiment but it is intrinsic to the measurement process. Indeed, the flow is lighted with a laser sheet (tomographic method) and therefore the third component of the displacement (out of plane component) is not taken into account. Both techniques do not allow the measurement of the third component but only the 2-D projection of the displacement. At the beginning of the experiment, the turbulence is very important and so the standard deviation of displacements is strongly underestimated.

To overcome this problem, there are two kinds of approach. First, it is possible to use stereoscopic system of PIV (known as 3 components PIV). The principle is to illuminate the flow with tomographic method and to acquire two images of the particles from two different viewpoints. Then, it is possible to determinate the three components of the displacements inside the laser sheet (obviously, the third component should not be important to allow the measurement). Stereoscopic PIV systems are now available commercially. The interested reader will find more information about this method in Riou (1999) and Prasad and Adrian (1993) for example. The second approach, known as three dimensional PIV, consists in lighting a volume in the flow. Then, the 3-D position of each particle is localized, through the calibration of cameras and conditions such as the epipolar geometry. Finally, the particles are tracked across successive images to measure the displacements. The main drawbacks of this approach is to need the localization of individual particles and therefore this limits the possible concentration.

7. Conclusion

In this paper, we have tested an alternative to cross-correlation method for determining velocity field from PIV images: the identification method. We extract the main characteristics of this algorithm: properties and sensibility to PIV parameters.

On the whole, this method is robust. However, the realized comparisons show that the cross correlation is more robust in many cases. But the displacement identification has some advantages compared with those of cross-correlation:

- its ability to measure the displacement in presence of light deviation or a piece of the facilities edges (Figs. 2 and 3),
- no link with the particle size (Fig. 4),
- ability to measure the velocity distribution in addition to the average velocity (Fig. 5).

Moreover, the effect on the identification method of particle concentration and noise is weak (Figs. 8, 9 and 15). For other parameters, we conclude that the identification gives good results in the following cases :

- the rate of isolated particles is not abnormally high, i.e. greater than 70% (Fig. 10),
- displacements are smaller than the half size of the interrogation cell, in the worst case (Fig. 11),
- velocity gradients are weak, i.e. less 13% of the average displacement (Figs. 12 and 13).

Comparisons with cross correlation and the application shown prove that this method is useful for real experiments. Indeed, the turbulence intensity decrease obtained thanks to identification is smoother and closer to the empirical one than to cross correlation measurements.

Acknowledgments

This work has been performed under the EUROPIV project. EUROPIV (a cooperative action to apply Particle Image Velocimetry to problems of industrial interest) is a collaboration between LML URA CNRS 1441, DASSAULT AVIATION, DASA, SIREHNA, CIRA, DLR, DRA, FFA, INTA, ISL, NLR, ONERA, VKI and the universities of Delft, Madrid, Oldenburg, Rome, Rouen (CORIA URA CNRS 230), St Etienne (TSI URA CNRS 842), Warwick. The project is managed by LML URA CNRS 1441 and is funded by the CEC under the IMT initiative (CONTRACT No.: BR.PR - CT95- 0118).

References

Adrian, R. J., Particle-imaging techniques for experimental fluid mechanics, Ann. Rev. Fluid Mech., 23 (1991), 261-304.

Comte Bellot G. and Corrsin S., The use of a contraction to improve the isotropy of a grid generated turbulence, J. of Fluid Mech., 25 (1966), 657.

Fayolle, J. et al., Displacements identification in particle image velocimetry, Compte Rendu à l'Academie des Sciences, t. 321, IIb, No.7, 273-278, (1995).

Fayolle, J., Study of images processing algorithms for the motion determination of unrigid objects, application to displacement determination in flows, PhD thesis, Univ. of Saint-Etienne, (1996).

Grant, I. and Liu, A., Accuracy considerations in incoherent analysis of PIV images, Applied Optics, 28-21 (1989), 4508-4510.

Keane, R. D. and Adrian, R. J., Theory of cross-correlation analysis of PIV images, Applied Scientific Research, 49 (1992), 191-215.

Okuno, T. and Kinoshita, T., A method of velocity field measurement using flow images, Proc. of the 4th Osaka symposium on flow measurement techniques (Osaka, Japan), (1987), 161-172.

Okuno, T., Some examples of image measurement in two dimensional flow field, Proc. of FLUCOME'91, (1991a), 623-628.

Okuno, T.,Velocity field measurement by flow images with Fourier transformation, J. of Kansai Shipbuilding Assoc., No.215 (1991b), 69-74.

Prabel, F., Study of jet turbulent structure of a circular jet by image analysis methods, PhD thesis, ECL Lyon, France, (1985).

Prasad, A. K. et al., Effect of resolution on the speed and accuracy of PIV interrogation, Exp. in Fluids, 13 (1992), 105-116.

Prasad, A. K. and Adrian, R. J., Stereoscopic particle image velocimetry applied to liquid flows, Exp. in Fluids, 15 (1993), 49-60.

Riou, L., Calibration methods of a stereoscopic system designed for flow displacement measurement in 2D and 3D, Ph.D. thesis, University of Saint-Etienne, France, (1999).

Rouland, E., Study and development of particle image cross-correlation. Application to hydrodynamic tunnel flows, PhD thesis, Rouen University, (1994).

Spiegel, M. R., Elementary sampling theory, (1961), 141-144, Schaum publishing Co, New York.

Author Profile

Jacques Fayolle: He received his postgraduate diploma “Images” in 1993 and the PhD degree of “Image analysis and image processing” in 1996 from the Saint-Etienne university. He is currently an assistant professor at the Institut Universitaire Professionnalisant Télécommunications and at the research laboratory, Traitement du Signal et Instrumentation - UMR CNRS 5516 at Saint-Etienne.
His current research interests include the determination of motion or deformation by image processing applied to fluid mechanics and to biomechanics. Others interest fields are pattern recognition through feature points characterization, camera calibration, segmentation of fuzzy objects, and the applications of the continuous wavelet transform. The main application of his research is the determination of displacements in turbulent flows or of some targets on human body.

Thierry Fournel: He is an assistant professor at the Technology Institute of Jean Monnet University (Saint-Etienne, France). Since 1989, he works as researcher in the Laboratory "Traitement du Signal et Instrumentation". His current research topics concern the development and the calibration of Stereoscopic Digital Particle Image Velocimetry (SDPIV) systems.

Philippe Gervais: He obtained his PhD in Energy Sciences at the "Falculté des sciences de Paris" in 1984. He is an assistant professor at Institut National des Sciences Appliquées of Lyon, France. His major research areas concern impinging jets and convection heat transfer problems for low velocity airflows. These topics are experimentally covered with laser visualization technique and have been resulted in PIV tools desing. His current research activities deal with development of thermal diffusivity measurement apparatus using both flash and harmonic techniques, respectively for low (130K to 400K) and high (500 to 3000) temperatures. From September 1998 to July 1999, he had been working as an invited professor in the Department of Chemical Engineering at McGill University at Montreal, Canada.